Enhanced regional terrestrial carbon uptake over South Korea revealed by atmospheric CO_2 measurements from 1999 to 2017

Running head: Terrestrial carbon cycle from atmosphere

Jeongmin Yun[1], Su-Jong Jeong[2*], Chang-Hoi Ho[1], Hoonyoung Park[2], Junjie Liu[3], Stephen Sitch[4], Pierre Friedlingstein[5], Sebastian Lienert[6], Danica Lombardozzi[7], Vanessa Haverd[8], Atual Jain[9], Sönke Zaehle[10], Etsushi Kato[11], Hanqin Tian[12], Nicolas Vuichard[13], Andy Wiltshire[14], Ning Zeng[15]

[1]School of Earth and Environmental Sciences, Seoul National University, Seoul, Korea

[2]Department of Environmental Planning, Graduate School of Environmental Studies, Seoul National University, Seoul, Korea

[3]Jet Propulsion Laboratory, California institute of Technology, Pasadena, CA 91109, USA

[4]College of Life and Environmental Sciences, University of Exeter, Exeter EX4 4RJ, UK

[5]College of Engineering, Mathematics and Physical Sciences, University of Exeter, Exeter 4QF, UK

[6]Climate and Environmental Physics, Physics Institute and Oeschger Centre for Climate Change Research, University of Bern, Bern, Switzerland

[7]National Center for Atmospheric Research, Boulder, Climate and Global Dynamics, Terrestrial Sciences Section, Boulder, CO 80305, USA

[8]CSIRO Oceans and Atmosphere, Canberra, ACT 2601, Australia

[9]Department of Atmospheric Sciences, University of Illinois, Urbana, IL, USA

[10]Biogeochemical Integration Department, Max Planck Institute for Biogeochemistry, 07745 Jena, Germany

[11]Research & Development Division, Institute of Applied Energy (IAE), Tokyo 105-0003, Japan

[12]School of Forestry and Wildlife Sciences, Auburn University, 602 Duncan Drive, Auburn, AL 36849, USA

[13]Laboratoire des Sciences du Climat et de l'Environnement, Institut Pierre-Simon Laplace, CEA-CNRS-UVSQ, CE Orme des Merisiers, 91191 Gif-sur-Yvette CEDEX, France

[14]Met Office Hadley Centre, FitzRoy Road, Exeter EX1 3PB, UK

[15]Department of Atmospheric and Oceanic Science and Earth System Science, Interdisciplinary Center, University of Maryland, College Park, Maryland, USA

Global Change Biology

(Primary Research Article)

*Corresponding author: Prof. Su-Jong Jeong (+82-2-880-5664; sujong@snu.ac.kr)

Keywords: carbon cycle, atmospheric CO_2 measurements, terrestrial ecosystems, terrestrial carbon fluxes, South Korea, satellite-measured NDVI, TRENDY, CT2017, GEOS-Chem

Abstract

The exact assessment of the role of terrestrial carbon balance in the regional carbon cycle is critical for understanding climate change. However, the lack of local measurements limits our knowledge of the regional-scale terrestrial carbon cycle. This study explored changes in the regional-scale terrestrial carbon cycle over South Korea by utilizing long-term atmospheric CO_2 measurements for the period 1999–2017. The influence of the regional land surface CO_2 fluxes on atmospheric CO_2 was estimated from the difference between the CO_2 concentrations (ΔCO_2) for two major wind directions: wind from the land sector and wind from the ocean sector. We found a significant decreasing trend in ΔCO_2 of 4.75 ppmv decade^{-1} ($p < 0.05$) during the growing season (May through October) suggesting that the regional land carbon uptake increased relative to the surrounding ocean areas. For the same period, the satellite-observed normalized difference vegetation index increased by 0.03 decade^{-1} across 90% of the South Korean territory; this accounts for a 4% increase. In line with the observed nationwide greening trend, satellite-measured gross primary production increased by 65.1 gC m^{-2} decade^{-1} over 93.9% of the region, accounting for a 8% increase. Both process-based terrestrial model and inversion model simulations estimated that the vegetation increase would lead to an enhancement of terrestrial carbon uptake by up to 101.3 gC m^{-2} decade^{-1}. Chemical transport model simulations showed that the observed ΔCO_2 decrease is associated with the enhancement of terrestrial carbon uptake rather than changes in anthropogenic emissions and atmospheric circulations. Based on the multiple lines of evidence from surface observations, satellite data, and modeling, our results suggest that the terrestrial carbon uptake over South Korea has been enhanced during the growing season for the recent two decades. These findings highlight the fact that atmospheric CO_2 measurements could open up the possibility of detecting regional changes in the terrestrial carbon cycle in data-limited environments.

Introduction

Atmospheric CO_2 concentration has risen from 278 parts per million by volume (ppmv) in pre-industrial times (1750) (Joos & Spahni, 2008) to 405 ppmv in 2017 (Dlugokencky & Tans, 2019) due to anthropogenic carbon emissions. Elevated atmospheric CO_2 increases the global mean temperature, which contributes to changes in the magnitudes and intensities of extreme weather events such as heat waves, droughts, and heavy rainfall (Min, Zhang, Zwiers, & Hegerl, 2011; IPCC, 2014; Seneviratne, Donat, Pitman, Knutti, & Wilby, 2016). Thus, a clear understanding of the carbon cycle is critical for recognition of contemporary climate change as well as future climate projections. The Global Carbon Project (GCP) (http://www.globalcarbonproject.org/), an international research project, estimates the annual global carbon budget using the latest models and observations to identify the processes that contribute to atmospheric CO_2 changes (Le Quéré et al., 2018). As a counterpart of GCP, the REgional Carbon Cycle Assessment and Processes project (RECCAP; Canadell et al., 2011) quantifies carbon fluxes on subcontinental scales. GCP estimated that around 5% of imbalance existed in the recent global carbon budget (Le Quéré et al., 2018). In line with GCP estimations, RECCAP highlighted significant uncertainties in the regional carbon budget (Huntzinger et al., 2012; Piao et al., 2013, Sitch et al., 2015; Thompson et al., 2016), implying limitations in our knowledge about spatiotemporal variations of the regional carbon cycle. Therefore, comprehensive analysis and assessment of the regional carbon cycle, including anthropogenic carbon emissions and land surface carbon balance, could reduce uncertainties in the global carbon cycle.

Terrestrial ecosystems alleviated the increasing atmospheric CO_2 by absorbing

91 approximately one third of emitted anthropogenic carbon from fossil fuel combustion and land
92 use change in 2017 (Le Quéré et al., 2018). Due to the high capability of carbon assimilation,
93 terrestrial ecosystems are considered one of the main components of the regional carbon cycle.
94 However, lack of relevant information on its spatial distribution and temporal variation has
95 made it difficult to assess changes in the terrestrial carbon sink. To estimate the changes,
96 previous studies have utilized process-based land surface models (e.g. Piao et al., 2011; Cui et
97 al., 2014; Lee et al., 2014; Yue, Unger, & Zheng, 2015), inverse modeling approach (e.g. Enting
98 and Mansbridge, 1989; Gurney et al., 2003; Nassar et al., 2011; Liu et al., 2014), forest
99 inventories (e.g. Choi, Lee, & Chang, 2002; Pan et al., 2011; Jeong et al., 2013; Fang et al.,
100 2014), and eddy covariance tower measurements (e.g. Piao et al., 2008; Dragoni et al., 2011;
101 Keenan et al., 2014; Yun & Chun, 2018). Process-based models are useful for estimating
102 responses of terrestrial ecosystems to environmental change on regional to global scales, but
103 they have inherent uncertainties. While inverse modeling frameworks help to reduce the
104 uncertainties in flux estimation by using atmospheric CO_2 measurements, the inversion results
105 are highly sensitive to the distribution of observation sites (Bruhwiler, Michalak, and Tans,
106 2011) and physical parameterizations in transport models (Patra et al., 2008; Peylin et al., 2013).
107 National forest inventories give reliable quantitative information on forest biomass changes,
108 but parameter uncertainties also occur when estimating forest carbon stock. Flux tower
109 measurements directly observe terrestrial carbon exchange with the atmosphere and yet the
110 number of measurement sites is insufficient for detecting regional-scale changes due to the
111 large spatial heterogeneity. Recently, new approaches have been introduced to overcome the
112 limitations of ground-based observations and models (Parazoo et al., 2016; Commane et al.,
113 2017, Jeong et al., 2018). For example, the study by Jeong et al. (2018) showed that the
114 ecosystem in the northern Alaska region has become a carbon source during autumn by
115 separating regional influence on atmospheric CO_2 at Barrow from the background. As such,

previous studies have shown that long-term atmospheric CO_2 observations could help us to evaluate the role of specific components, such as terrestrial ecosystems, in determining atmospheric CO_2 concentrations in data-limited environments.

South Korea (Republic of Korea), located in East Asia, has been experiencing rapid economic development and land-use change over recent decades. Accelerated industrialization and urbanization since the 1970s has more than tripled the gross domestic product between 1999 and 2017 (World Bank, 2018). With this economic growth, there is an associated increase in the consumption of energy, that is predominantly supplied by fossil fuels, making South Korea the 9th largest fossil fuel CO_2 emitter in the world in 2017 (168 Tg C $year^{-1}$; Global Carbon Project, 2018). Thus, South Korea is likely a hot-spot of carbon emissions. In contrast to the large emissions is the carbon sink across the country, which has changed considerably over the recent decades. A national plan of reforestation and forest management was implemented in 1973. Sustained forest management by the national forestry department and the local governments has increased the volume of forests in Korea from 60.3 m^3 ha^{-1} in 1999 to 146.0 m^3 ha^{-1} in 2015 (Korea Forest Service, 2018). The managed young forests, occupying around 65% of the country, had the highest carbon sequestration rate over East Asia of 5 ~ 12 Tg C $year^{-1}$ in the 1990s and 2000s (Choi et al., 2002; Li, Yi, Son, Jin, & Han, 2010) and have potentially offset 8.9% of the domestic anthropogenic emissions from the 1970s to 2000s (Fang et al., 2014). Furthermore, a longer vegetation growing season related to regional warming could contribute to enhancing carbon sequestration over South Korea (Jeong et al., 2013). Therefore, assessing the role of terrestrial ecosystem change in the regional carbon cycle is critical to understanding the carbon cycle dynamics.

Continuous monitoring of atmospheric CO_2 concentrations has been ongoing in South Korea at Anmyeondo (AMY) since 1999. The AMY site is located on the western tip of the Korean Peninsula, which is surrounded by the ocean on three sides and has the advantage of being able to monitor variations in atmospheric CO_2 both within and outside the mainland. Using the long-term measurements at the AMY site, the present study assessed the possibility of using atmospheric CO_2 measurements to understand the terrestrial carbon cycle at a regional scale (i.e. South Korea). We first estimated the influence of the regional land surface on atmospheric CO_2 from the difference between CO_2 concentration values during wind from the land sector and wind from the ocean sector, which can be considered a proxy for the net ecosystem exchange, as in Jeong et al. (2018). To further explain the observed regional changes in atmospheric CO_2, we identified changes in vegetation and terrestrial carbon fluxes using satellite measurement datasets and model simulation results, respectively. The influences of changes in regional land-surface carbon fluxes as well as atmospheric transport on the CO_2 concentration were also evaluated through the chemical transport model simulations. Based on multiple lines of evidence, this study provides reliable information on changes in the terrestrial carbon cycle over South Korea during the last two decades.

Materials and methods

This study combines both observation analysis and model simulations to investigate changes in the terrestrial carbon cycle over South Korea in the last two decades. We first estimated the changes in regional land-surface CO_2 fluxes from the difference between CO_2 concentration measured at AMY Station when wind blows from the land sector and when wind blows from the ocean sector (i.e. ΔCO_2). We assumed that the observed ΔCO_2 trend is associated with changes in the regional terrestrial carbon fluxes and identified changes in vegetation and

terrestrial carbon fluxes in the region. The changes in vegetation and vegetation activity (i.e. photosynthesis) were investigated using the GIMMS and MODIS NDVI datasets and MODIS GPP dataset, respectively. The changes in terrestrial carbon fluxes were estimated using the TRENDY model simulation results and the CT2017 dataset. To verify our assumption, we conducted GEOS-Chem model simulations to evaluate the influences of changes in regional terrestrial carbon fluxes as well as fossil fuel carbon emissions and atmospheric circulation on the CO_2 concentration over South Korea.

Atmospheric CO_2 observation

The Anmyeondo Observatory (36.53°N, 126.32°E) is one of 111 World Meteorological Organization (WMO) Global Atmosphere Watch (GAW) regional stations (Figure 1). The Korea Meteorological Administration (KMA) has continuously measured atmospheric CO_2 concentrations at the site from a 40 m tower (47 m above sea level) since January 1999 (Cho, Kim, & Yoo, 2007; Lee, Han, Ryoo, Lee, & Lee, 2019). The collected data is managed by the World Data Centre for Greenhouse Gases (WDCGG; https://gaw.kishou.go.jp/). We used hourly CO_2 concentration data from January 1999 to October 2017, which were calibrated through quality control processes reported in Lee et al. (2019). The reliability of the hourly data was evaluated by comparison with flask-air samples collected weekly at the AMY Station (Lee et al., 2019).

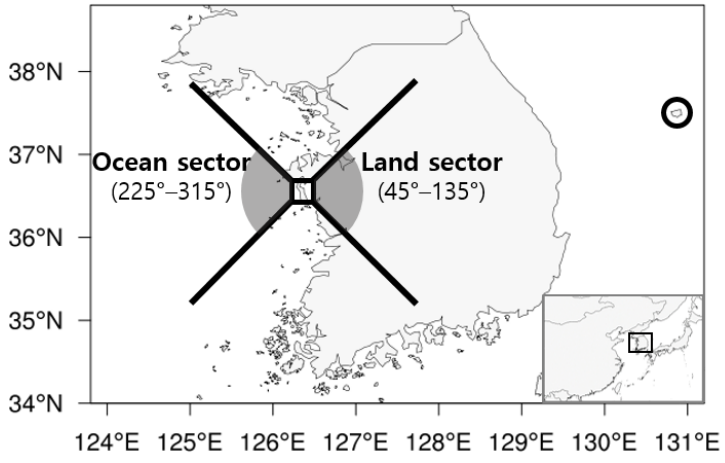

184

185 **Figure 1** Locations of Anmyeondo (AMY; open box) and Ulleungdo Observatories (ULD;
186 open circle) and position of the ocean sector and the land sector with respect to AMY. The
187 ocean sector is defined as the region where wind blows from 225–315° and the land sector is
188 defined as the region where wind blows from 45–135° with respect to AMY. The inset figure
189 shows the location of South Korea over East Asia.

190

191 Influences of regional land surface CO_2 fluxes on atmospheric CO_2 were distinguished
192 based on wind speed and direction. Due to absence of local wind data, we used hourly wind
193 data from the Automated Synoptic Observing System at Seosan Station, which is the wind
194 measurement site nearest to the AMY Station (around 30 km). To reduce the effect of local
195 sources and expand the area of influence, we only considered the hourly CO_2 data with wind
196 speeds exceeding 3 m s^{-1} during the daytime (from 12:00 p.m. to 17:00 p.m.) when vertical
197 mixing is active. Our main findings are identical when the threshold is between 2.5 and 3.5 m
198 s^{-1}. The wind direction at Seosan Station has been recorded using 16 directions with 22.5°
199 spacing. Taking into account the coastline layout, regionally influenced CO_2 concentration
200 (CO_2^{land}) was defined as observations made when the wind direction is between 45° and 135°
201 (land sector). Background CO_2 concentration for the CO_2^{land} (CO_2^{ocean}) was defined as

observations made when the wind direction is between 225° and 315° (ocean sector). The wider ranges of wind direction did not alter our results, but we aimed to discriminate between CO_2^{land} and CO_2^{ocean}. The separated CO_2^{land} and CO_2^{ocean} were smoothed by the curve-fitting method of Thoning et al. (1989) and aggregated into monthly values. We treat the difference between the monthly CO_2^{land} and CO_2^{ocean} (ΔCO_2 = CO_2^{land} minus CO_2^{ocean}) as a proxy for the atmospheric signal for regional land-surface CO_2 fluxes over South Korea. This approach has been applied to determine the changes in regional CH_4 and CO_2 exchange (Sweeney et al., 2016, Commane et al., 2017, Jeong et al., 2018).

The KMA has also been monitoring atmospheric CO_2 at Ulleungdo (ULD; 37.48°N, 130.90°E) from a 10 m tower (221 m above sea level) with the same measurement system of Anmyeondo (AMY) station since 2014 after two years of test operation (Lee et al., 2019). The ULD site is located at Ulleung-do (72 km^2), around 155 km east from the mainland (Figure 1), and data from this site represents the atmospheric CO_2 flowing into the mainland from the East Sea. Hourly CO_2 concentrations at the ULD site is used to compare with the CO_2^{land} for validating whether the variations of CO_2^{land} are attributed to the regional land-surface CO_2 fluxes or the air coming from the East Sea. The hourly ULD CO_2 concentration data is smoothed by the curve-fitting method of Thoning et al. (1989) and aggregated into monthly values from January 2014 to October 2017 to compare with the CO_2^{land}.

Back-trajectory analysis

To verify our classification between CO_2^{land} and CO_2^{ocean}, we investigated directions of air mass inflow for winds from the land sector and ocean sector using a back-trajectory model. We

used the National Oceanic and Atmospheric Administration (NOAA) HYbrid Single-Particle Lagrangian Integrated (HYSPLIT, version 4; Stein et al., 2015) model to calculate 48-h back-trajectories of air masses arriving at the AMY Station. The trajectories started at 500 m above sea level, which are within the height of the mixing layer for daytime. The National Centers for Environmental Prediction/National Center for Atmospheric Research (NCEP/NCAR) reanalysis meteorological dataset with a 6-h interval and spatial resolution of 2.5° was used as the model input. To investigate the overall spatial patterns of the trajectories for each case, we generated trajectory densities of the air masses at a 0.5° x 0.5° spatial resolution. We then calculated the percentage of the number of trajectories passing through each grid cell among the total number of back-trajectories and the median trajectory at 6-h endpoints for each case. Altering the start altitude level from 500 m to 1000 m did not change results in this study (not shown here).

Satellite-measured NDVI dataset

Remote sensing provides continuous observational data over vast areas. Satellite-measured normalized difference vegetation index (NDVI) datasets have been widely used to detect variations in vegetation growth (e.g. Jeong, Ho, & Jeong, 2009; Jeong et al., 2013; Zhang, Song, Band, Sun, & Li, 2017). Here we used two different satellite-measured NDVI datasets, the Global Inventory Monitoring and Modeling System (GIMMS) 3g NDVI and Moderate Resolution Imaging Spectroradiometer (MODIS) NDVI, to gather more reliable information on the changes in vegetation over South Korea during the last two decades.

The third generation of the GIMMS NDVI dataset was produced from advanced very high-

248 resolution radiometers (AVHRRs) on the polar-orbiting meteorological satellites of NOAA and
249 European organizations for the exploitation of meteorological satellites (Pinzon & Tucker,
250 2014; data available at https://ecocast.arc.nasa.gov/data/pub/gimms/3g.v1). The dataset was
251 calibrated using the Bayesian method and other satellite-measured NDVI data derived from the
252 Sea-Viewing Wide Field-of-view Sensor. The reported accuracy of the data is within ± 0.005
253 (Pinzon & Tucker, 2014). The GIMMS NDVI dataset covers the period from July 1981 to
254 December 2015 with a 1/12 degree of spatial resolution and 15-day intervals. The data for the
255 period overlapping (i.e. from 1999 to 2015) with the AMY CO_2 data collection period was used
256 for the current study.

257

258 The MODIS NDVI dataset from MOD13C1 (Version 6) products was derived from
259 MODIS Terra images (Didan, 2015). The MOD13C1 dataset is spatially aggregated from 1
260 km of cloud-free MOD13A2 data to a 0.05° geographic climate modeling grid with 16-day
261 intervals, and covers the period from February 2000 to present (data available at
262 https://lpdaac.usgs.gov/products/mod13c1v006/). Reliability of the MODIS NDVI dataset was
263 evaluated by comparisons with other existing satellite-measured NDVI data and its accuracy is
264 within ± 0.025 (MODIS Land Team, 2018). The data for the period overlapping (i.e. from 2000
265 to 2017) with the AMY CO_2 data collection period was used for the current study.

266

267 *MODIS GPP*

268 The MODIS gross primary production (GPP) dataset from MOD17A2H (Version 6)
269 products from MODIS Aqua and Terra images were used to estimate the changes in GPP in
270 South Korea from 2000 to 2017 (Running and Zhao, 2015). The algorithm based on light use

efficiency concepts was applied to generate the GPP dataset from the meteorological field of the Global Modeling and Assimilation Office supported by the National Aeronautics and Space Administration and satellite-derived fraction of photosynthetically active radiation from MOD15 (Running and Zhao, 2015). The MOD17A2H dataset is a cumulative 8-day composite of values with 500m spatial resolution, and covers the period from February 2000 to present (data available at https://lpdaac.usgs.gov/products/mod17a2hv006/). The MODIS GPP dataset was spatially aggregated from 500 m to a 0.05° geographic climate modeling grid to match spatial resolution of MODIS NDVI for the current study.

TRENDY models

We used monthly averaged carbon fluxes (GPP, Ra; autotrophic respiration, Rh; heterotrophic respiration, and NBP; net biome production) simulated by 11 dynamic global vegetation models from the TRENDY project version 6 (S3 simulation; Sitch et al., 2015) to estimate changes in terrestrial carbon fluxes over South Korea between 2000–2016. The list of the models used are as follows: CABLE (Haverd et al., 2018), CLM4.5 (Oleson et al., 2013), DLEM (Tian et al., 2015), ISAM (Jain, Meiyappan, Song, & House, 2013), LPJ (Sitch et al., 2003), LPX-Bern (Stocker, Feissli, Strassmann, Spahni, & Joos, 2014), OCN (Zaehle, Friedlingstein, & Friend, 2010), ORCHIDEE (Krinner et al., 2005), VEGAS (Zeng, Mariotti, & Wetzel, 2005), VISIT (Ito & Inatomi, 2012), and JULES (Clark et al., 2011). Models were forced by observed climate fields from the Climate Research Unit (CRU) dataset (e.g. CRU-TS 3.23 and 3.25) or CRU-National Centers for Environmental Prediction version 8 meteorological dataset, global atmospheric CO_2 concentration data from ice-cores and atmosphere measurements from NOAA Earth System Research Laboratory (ESRL) (Dlugokencky & Tans, 2019), and land-use and land cover change data from the Hyde database (Hurtt et al., 2011). The model outputs from the TRENDY project have been applied in a

number of studies to estimate the changes in terrestrial carbon balance and to understand driving factors for the change at global as well as regional scales (e.g. Piao et al., 2012; Le Quéré et al., 2018).

GEOS-Chem model simulations

We used the Goddard Earth Observing System (GEOS)-Chem model, a global 3-D chemical transport model (CTM) for atmospheric compositions (Bey et al., 2001), to evaluate the influences of changes in the regional land-surface carbon fluxes and atmospheric transport on the CO_2 concentrations over South Korea. We conducted GEOS-Chem CO_2 simulations, which ignore the chemical reactions of CO_2 but consider surface CO_2 fluxes to the atmosphere and transport of atmospheric CO_2. This version of the model has been widely used to investigate the response of atmospheric CO_2 to changes in fossil fuel emissions (e.g. Nassar et al., 2013) and terrestrial carbon fluxes (e.g. Barnes, Parazoo, Orbe, & Denning, 2016, Parazoo et al., 2016).

We used a nested-grid GEOS-Chem model (version 11.2) with the native 0.5° x 0.667° horizontal resolution and 47 vertical layers from surface pressure to 0.01 hPa over East Asia (11°S–55°N, 70–150°E) (Wang, McElroy, Jacob, & Yantosca, 2004). Boundary conditions for the nested version of the model were provided hourly from the global GEOS-Chem simulations with 4° x 5° horizontal resolution. All model simulations were performed by using observed meteorological data and a surface CO_2 flux dataset. We used the 3-hourly meteorological data from Modern-Era Retrospective analysis for Research and Applications version 2 (MERRA-2) datasets with the same spatial resolutions as each simulation (Gelaro, et al., 2017). The surface

carbon flux dataset includes terrestrial biospheric exchange, ocean exchange (Takahashi et al., 2009), emissions from fossil fuels, biomass burning (Randerson, Van Der Werf, Giglio, Collatz, & Kasibhatla, 2018), biofuel burning (Yevich & Logan, 2001), shipping, and aviation (Simone, Stettker, & Barrett, 2013). From the carbon flux dataset, monthly terrestrial carbon fluxes and fossil fuel CO_2 emissions were taken from CarbonTracker outputs (CT2017; Peters et al. 2007 with updates documented at http://carbontracker.noaa.gov) and the Open-source Data Inventory for Anthropogenic CO_2 (ODIAC) dataset (Oda & Maksyutov, 2011), respectively.

GEOS-Chem was spun up from 1990 to 1999 using the meteorological data and fossil fuel data of 1990–1999 and the other surface CO_2 flux datasets fixed at their values of the year 2000. Starting from the model state in 2000, we performed a set of sensitivity simulations for 2000–2016 (Table 1). In the E1 simulation, all variables used were transient. In the E2, E3, and E4 simulations, one or both monthly terrestrial carbon fluxes and fossil fuel carbon emissions in 2000 were repeatedly prescribed over South Korea (34–38°N, 126–130°E) during the entire simulation period, respectively, but other conditions were identical to those of the E1 simulation. The E5 simulation is identical to the E3 simulation, but the carbon emissions in 2000 were prescribed over eastern China (20–40°N, 100–125°E and 40–50°N, 100–140°E) and not South Korea. From the difference between the E1 simulation and E2 and E3 simulations (e.g. E1 minus E2), influences of the changes in regional terrestrial carbon fluxes and carbon emissions on atmospheric CO_2 in South Korea were estimated, respectively. The possible influences of changes in transported atmospheric CO_2 from other regions were estimated in the E4 simulation. The effect of changes in carbon emissions in eastern China, which are expected to account for the largest portion of the transported CO_2, was estimated from the difference between the E1 simulation and E5 simulation. The model bias related to the overestimation of

343 the long-term trend in CO_2 concentrations was corrected by comparing the AMY CO_2
344 concentration data. Only surface CO_2 concentrations simulated from the model were used for
345 analysis in the study.

346

347 **Table 1** Set of model simulation to estimate the influences of changes in regional land-surface
348 carbon fluxes and transport on CO_2 concentrations over South Korea for the period 2000–2016.

Simulations	Descriptions	
	Terrestrial carbon flux	Fossil Fuel carbon emissions
E1	T	T
E2	South Korea FIX	T
E3	T	South Korea FIX
E4	South Korea FIX	South Korea FIX
E5	T	Eastern China FIX

T: all transient variables are used.
FIX: flux in 2000 were repeatedly prescribed over the region.

349

350

351 In the case of terrestrial carbon fluxes, we conducted an additional set of model simulations
352 using TRENDY model results. In the T1 simulation (i.e. control simulation), balanced monthly
353 terrestrial carbon flux (from SiB3 model; Messerschmidt et al., 2013) with climatological value
354 of annual terrestrial exchange (from TransCom models; Baker et al., 2006) were repeatedly
355 prescribed during the entire simulation period; there are no annual changes in the seasonal cycle
356 of the terrestrial carbon fluxes. In T2, T3, and T4 simulations (i.e. sensitivity simulations), the
357 monthly flux in South Korea is set to linearly change from the balanced value by the average,
358 maximum, and minimum trends of the estimated NBP in the TRENDY models during the entire
359 simulation period. The range of influences of change in NBP on the CO_2 concentrations,
360 estimated by TRENDY models, are obtained from the differences of T2, T3, and T4 simulations

with the T1 simulation,

Results

Comparison of the back-trajectories of air masses between the land and ocean sectors

Our method for distinguishing the regional influence on atmospheric CO_2 was first verified by back trajectory analysis. Figure 2 shows probability densities of 48-h trajectories ending at the AMY Station at 500 m altitude. The percentage decreases farther away from the station with a value of 100%, which indicates that all trajectories pass the area. Trajectory distributions of the air masses for wind from the ocean sector and land sector explicitly differ. To gather quantitative information, we set a domain centered at the station (35.5–37.5°N, 125.3–127.3°E; boxed area in Figure 2a) and noted which direction the air masses arrived from at the domain. 88.3% of the air mass for wind from the ocean sector enters the AMY Station from the ocean side (Figure 2a). The northwestern airflow is dominant, and it crosses the west coast of the Korean Peninsula. Conversely, 82.9% of the air mass for wind from the land sector enters the domain from the landside (Figure 2b). The main airflows arrive at the station directly from the east of the Korean Peninsula. The rest 17.1% of the air mass enters the domain from the ocean side, especially northwest of the Station. The mismatched air mass contributes to shifting the median of back-trajectories in the east coast of the Korean Peninsula toward the northeast between 36 and 48 hours prior. These trajectory patterns show that our wind direction-based classification is reasonable for separating of air mass into two groups: inflow from outside and inflow from inside the Korean Peninsula (i.e., CO_2^{ocean} and CO_2^{land}).

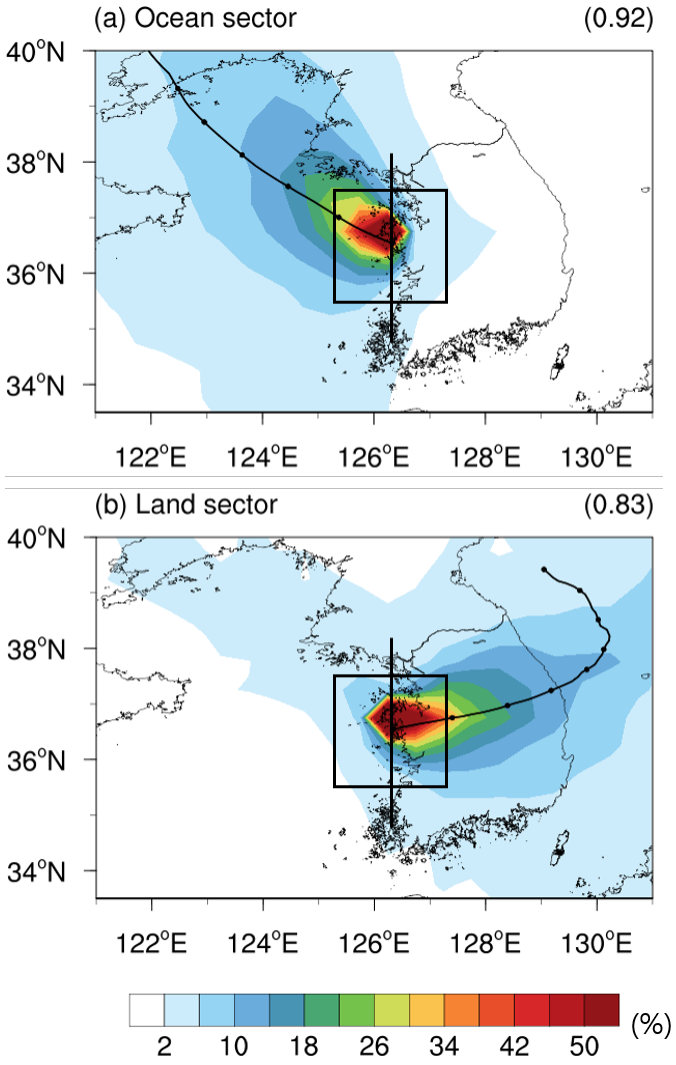

383

384 **Figure 2** Density plots for 48-h trajectories terminating at AMY at 500m altitude for wind from
385 (a) the ocean sector and (b) the land sector for the period 1999–2017. Solid line represents the
386 median trajectory. Markers on the trajectories represent the position of air masses at 6-hour
387 intervals. Upper-right numbers of each plot signify the ratio of air masses that came into the
388 domain (boxed area; 35.5–37.5°N, 125.3–127.3°E) from the ocean side among the total air
389 mass of wind from the ocean sector and vice versa.

390

391 *Comparison of the atmospheric CO_2 concentrations between Stations*

392 The possible influences of air coming from the East Sea of Korea were also assessed from

the comparison between CO_2 concentrations at land sector and ULD Station. On average, the CO_2 concentration at the ULD site is lower than both CO_2^{land} and CO_2^{ocean} by 2.2 and 3.2 ppm from January 2014 to October 2017 (Figure 3), respectively, because the ULD site is located far from the CO_2 source regions. However, the seasonal variability of CO_2^{land} is greater than that of the CO_2 concentrations at the ULD site and annual minimum value of the monthly CO_2^{land} is lower than that of the ULD site in three of the past four years. For example, in 2014, the annual maximum and minimum value of CO_2^{land} are 415.4 and 387.9 ppmv but those of the ULD CO_2 concentration are 407.4 and 396.2 ppmv, respectively. In addition, averaged CO_2^{land} from May to September (400.3 ppmv) is lower than that of the ULD CO_2 concentration (403.9 ppmv) by 3.6 ppmv during the analysis period. These results indicate that the variations of CO_2^{land} are mainly attributed to the regional land-surface CO_2 fluxes rather than the air coming from the East Sea.

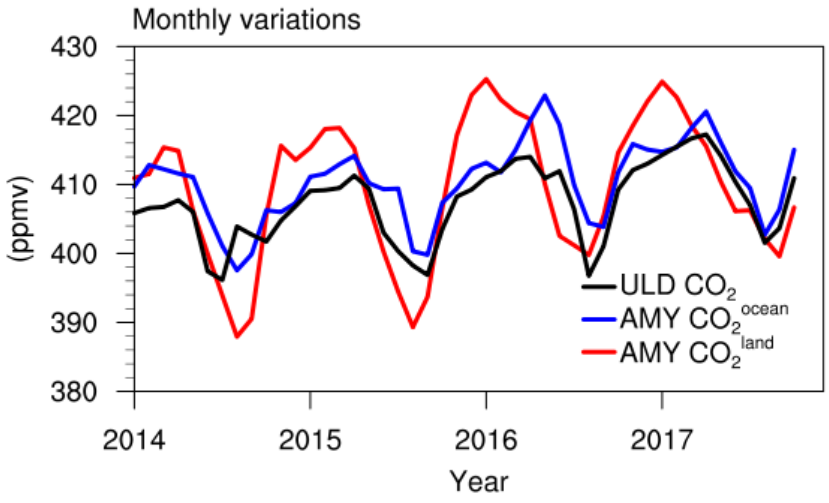

Figure 3 Monthly variations of atmospheric CO_2 at Ulleungdo station (ULD; black line) and CO_2 concentrations for wind from the ocean sector (CO_2^{ocean}; blue line) and land sector (CO_2^{land}; red line) at Anmyeondo station (AMY) from January 2014 to October 2017.

Regional influence on atmospheric CO_2 concentration variations

Both time series of CO_2^{land} and CO_2^{ocean} at the AMY Station show gradually increasing trends and clear seasonal variations, with the maximum in winter and minimum in summer from January 1999 to October 2017 (Figure 4a). However, the seasonal variability of CO_2^{land} is greater than that of CO_2^{ocean}. In comparison with CO_2^{ocean}, annually averaged CO_2^{land} is lower by 1.9 ppmv on average during the growing season (from May to October) and higher by 3.6 ppmv on average during the non-growing season (from November to April) for the total study period (Figure 4b; black thick line). The maximum value of the difference between CO_2^{land} and CO_2^{ocean} (i.e. ΔCO_2) is found in January at 6.1 ppmv and the minimum is exhibited in August at –3.5 ppmv.

Notable decreases in annually averaged ΔCO_2 during the growing season appear in recent years from 0.5 ± 2.1 ppmv in 1999–2006 to –5.0 ± 2.2 ppmv in 2010–2017 (Figure 4b; bar). Moreover, the annually averaged monthly ΔCO_2 in the two periods are out of each other's error ranges as represented by the 1σ in May, June, July, and September. For example, the annually averaged ΔCO_2 in May is 1.0 ± 3.0 ppmv in the first eight years and –4.8 ± 3.8 ppmv in the last eight years. A statistically significant decreasing trend of the ΔCO_2 is also observed for the growing season, on average, at 4.75 ppmv decade^{-1} ($p < 0.05$; Figure 4c). The maximum decreasing trend is exhibited in May at 6.39 ppmv decade^{-1} ($p < 0.05$) and the minimum is found in April at 1.81 ppmv decade^{-1}. An increase in the ΔCO_2 is observed from November to March at 1.27 ppmv decade^{-1} but this is not significant. The results suggest that the increase in atmospheric CO_2 concentration over South Korea is relatively lower than that in the surrounding ocean regions, especially during the growing season for the last two decades.

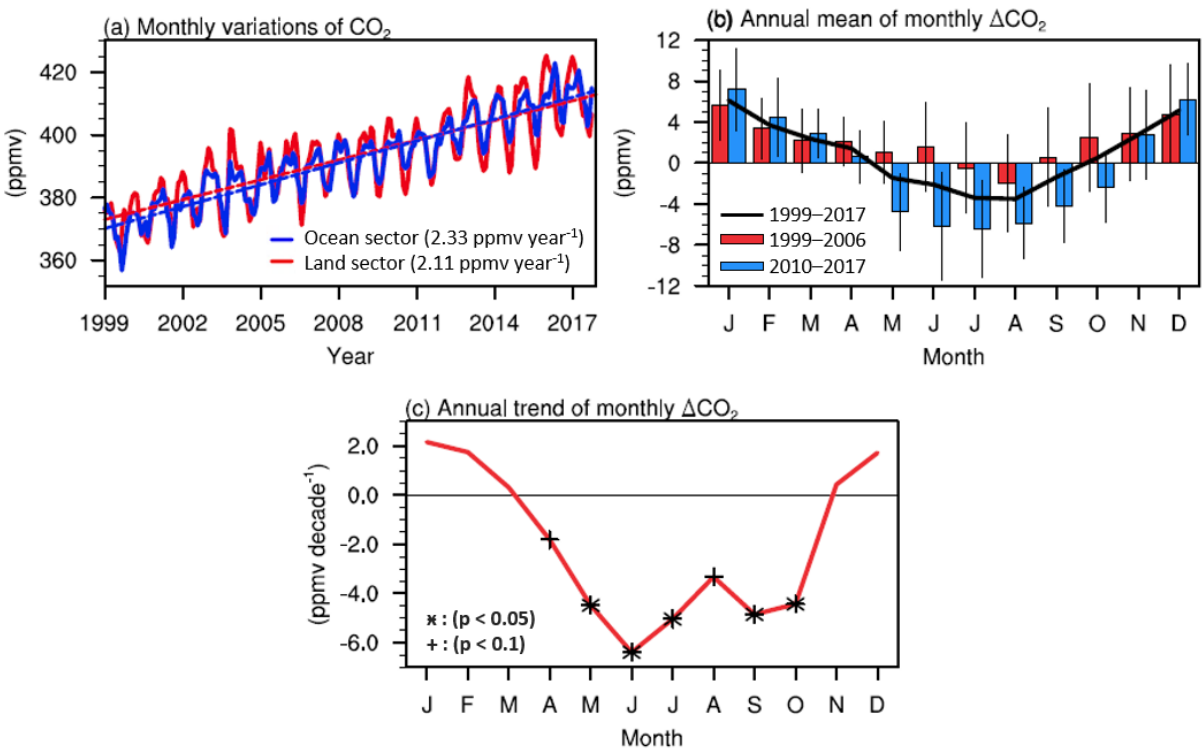

Figure 4 Variations of (a) monthly mean CO_2 concentrations for wind from the ocean sector (CO_2^{ocean}; blue line) and land sector (CO_2^{land}; red line) for the period 1999–2017. (b) Annually averaged monthly ΔCO_2 for the entire study period (black thick line), the first eight years (1999–2006; red bar), and the last eight years (2008–2017; blue bar). Error bar shows the monthly standard derivation of the ΔCO_2. (c) Trends of monthly mean ΔCO_2 for the same period. The asterisk and cross indicate statistical significance at the 95% and 90% confidence level, respectively.

Changes in vegetation and terrestrial carbon fluxes

To understand the reasons for the observed decreases in ΔCO_2 during the growing season, we investigated the changes in vegetation and terrestrial carbon fluxes over South Korea for the last two decades. South Korea, where two thirds of the country are forests (Korea Forest

Service, 2018), has a climatological NDVI of 0.69 (GIMMS: 0.69, MODIS: 0.69; Figure 5a, b) and an accumulated GPP of 919 gC m^{-2} during the growing season (Figure 5c). Both linear trends of NDVI from the two different satellite measurements show nationwide positive values (Figure 5a, b). For the growing season, the NDVI from GIMMS increased by 0.030 $decade^{-1}$ over 90.2% of South Korea from 1999 to 2015; this accounts for a 4.3% increase. Similarly, the NDVI from MODIS increased by 0.025 $decade^{-1}$ over 93.7% of the entire study area from 2000 to 2017; this accounts for a 3.6% increase. The greening trends of NDVI from GIMMS and MODIS are significant at the 95% confidence level in 34.0% and 75.1% of the study area, respectively. In line with the observed nationwide vegetation greening trend, accumulated GPP from MODIS increased by 65.1 gC m^{-2} $decade^{-1}$ over 93.9% of the entire study area during the growing season from 2000 to 2017; this accounts for a 7.6% increase (Figure 5c). Some parts of central South Korea show decreases or relatively small increases in the GPP, but a significant increase in the GPP is observed in 45.4% of the analysis domain, especially over the southwestern part of South Korea.

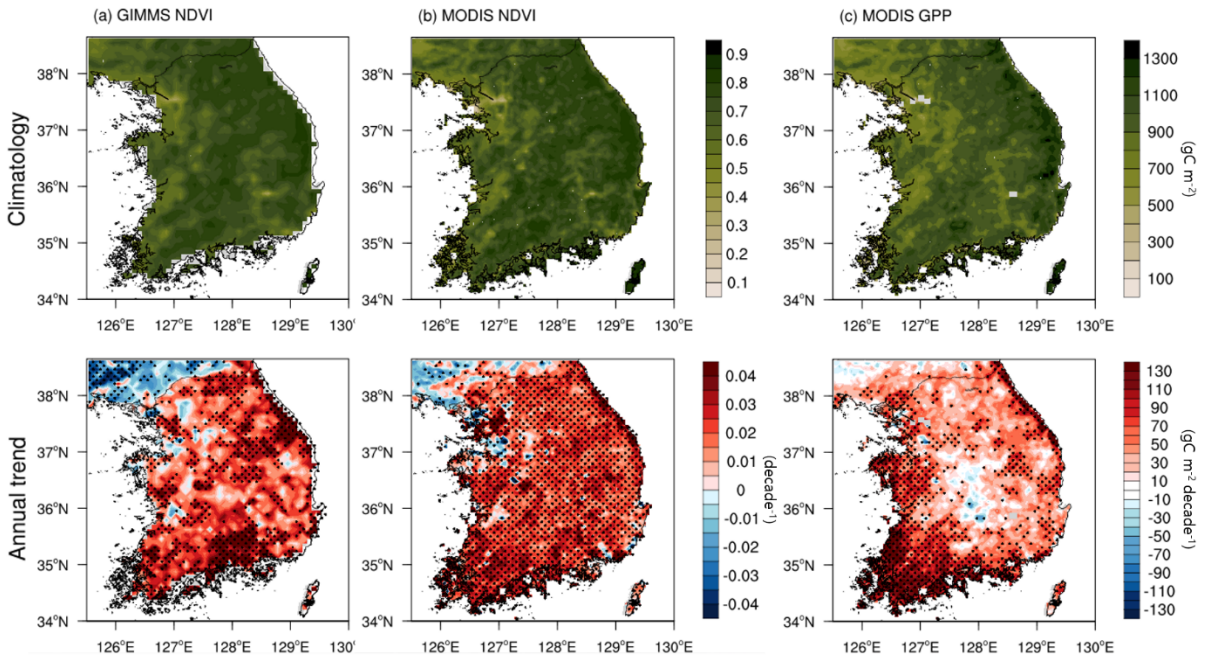

Figure 5 Spatial distributions of climatology and trends in averaged (a) GIMMS and (b) MODIS normalized difference vegetation index (NDVI) during the growing season (May through October) over the period 1999–2015 and 2000–2017, respectively. The stippled areas represent statistically significant correlations ($p < 0.05$). (c) Same as (b) but for accumulated gross primary production (GPP) from MODIS.

The TRENDY multi-model mean overestimated the climatology of the annual GPP average of the study area as 350 gC m^{-2}, but it estimated an increase in GPP for the growing season by 54.8 ± 27.5 gC m^{-2} $decade^{-1}$, similar to the GPP from MODIS (61.4 gC m^{-2} $decade^{-1}$) for 2000–2016 (Figure 6a). Due to the relatively low increase in total respiration (36.0 ± 29.0 gC m^{-2} $decade^{-1}$) compared with the GPP, the net terrestrial carbon uptake (i.e. NBP) increased by 18.5 ± 24.0 gC m^{-2} $decade^{-1}$ during the growing season; this accounts for 14.2 ± 18.5% of its climatological value (125 ± 105 gC m^{-2}) (Figure 6b, c). Even though large variations between the TRENDY models exist from -48.7 to 101.3 gC m^{-2} $decade^{-1}$ (this accounts for 39.0% of decrease and 81.0% of increase), the NBP from the multi-model mean has the same sign with the trends of the biospheric carbon flux of 42.9 gC m^{-2} $decade^{-1}$ from CT2017; this accounts for 45.5% of its climatological value (94.2 gC m^{-2}). Both TRENDY and CT2017 models estimate a relatively lower increasing trend of the carbon flux in July than adjacent months. This is due to the stagnant rain front created during summer rainy seasons which blocks solar radiation and inhibits vegetation growth over South Korea (Lee et al., 2017). These results suggest that the terrestrial carbon uptake in South Korea has increased during the growing season due to the nationwide vegetation greening trend for the last two decades.

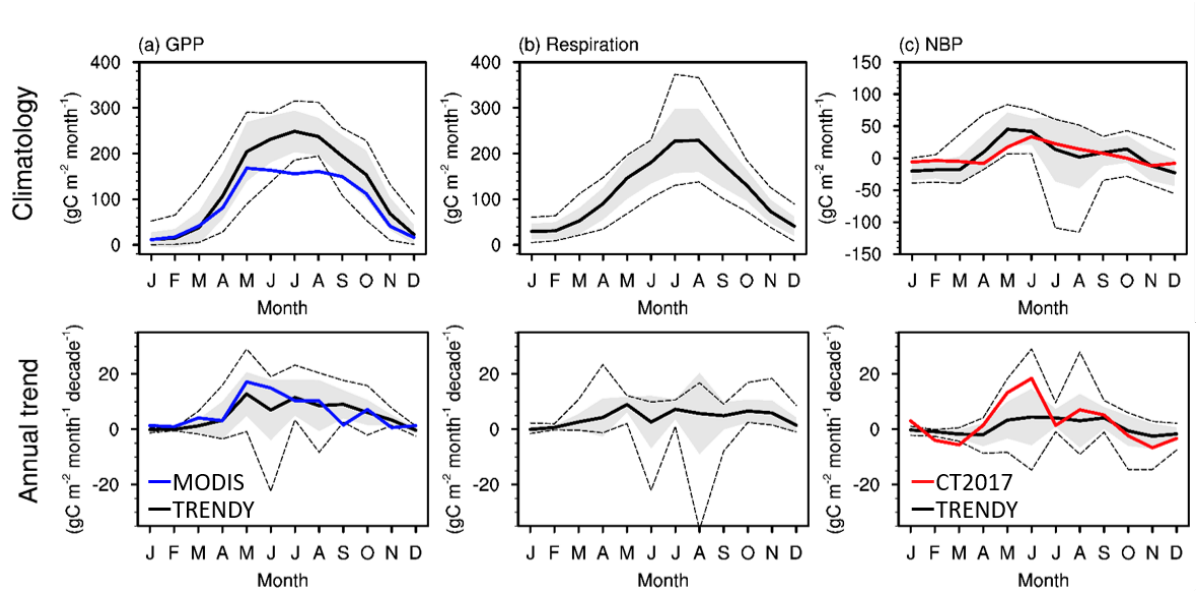

487

488 **Figure 6** Area-averaged climatology and trends in monthly (a) gross primary production (GPP),
489 (b) total respiration (i.e. autotrophic respiration + heterotrophic respiration), and (c) net biome
490 production (NBP) in South Korea according to simulations from TRENDY models (black line)
491 over the period 2000–2016. The shading denotes one inter-model standard deviation range
492 of each month. The dotted lines represent the minimum and maximum values of monthly
493 trends in the carbon fluxes estimated from TRENDY models. Blue and red lines indicate GPP
494 from MODIS and biosphere carbon flux from CT2017, respectively.

495

496 *Influences of changes in regional land-surface carbon fluxes on CO_2 concentrations*

497 We assessed the influence of model-estimated changes in regional terrestrial carbon
498 fluxes on CO_2 concentrations in South Korea (35–38°N, 126.5–129.5°E) from the CTM
499 simulations for the period 2000–2016. The increasing terrestrial carbon fluxes estimated in
500 both CT2017 and TRENDY multi-model mean consistently induced decreases in CO_2
501 concentrations in South Korea during the growing season, distinct from the non-growing
502 season (Figure 7a). The flux change estimated by the CT2017 decreased CO_2 concentration by

503 0.64 ppmv decade^{-1} during the growing season and caused little change in the CO_2
504 concentration by 0.06 ppmv decade^{-1} during the non-growing season (Figure 7a; red line). The
505 maximum decreasing trend appeared in June at 1.38 ppmv decade^{-1}, likewise with the ΔCO_2
506 trend. Even though the flux change estimated by the TRENDY multi-model mean induces a
507 relatively small decrease in the CO_2 concentration during the growing season (0.24 ppmv
508 decade^{-1}) than that from CT2017, the models estimated that the CO_2 concentration would
509 decrease at most by 1.38 ppmv decade^{-1} (Figure 7a; black line). A possible maximum
510 decreasing trend of the CO_2 concentration is also exhibited in June at 2.39 ppmv decade^{-1}. The
511 results suggest that the observed decreasing trend of ΔCO_2 is associated with the enhancement
512 of terrestrial carbon uptake in South Korea during the growing season for the study period.

513

514 In addition to the biosphere fluxes, anthropogenic carbon emissions increased by 33
515 Tg C decade^{-1} in South Korea for the analysis period. Seasonal differences in the monthly
516 carbon emissions trends also appear; the trends of the non-growing season (2.9 Tg C month^{-1}
517 decade^{-1}) is greater than that of the growing season (2.6 Tg C month^{-1} decade^{-1}) by 0.3 Tg C
518 month^{-1} decade^{-1} on average; this accounts for around 12% of the annual mean trends. The
519 possible influence of the increasing carbon emissions was also evaluated. Our model estimates
520 that the rise of domestic carbon emissions increases annual mean CO_2 concentrations in South
521 Korea by 1.11 ppmv decade^{-1} (Figure 7b). However, notable seasonal differences are not
522 observed in the increasing trends; the seasonally averaged trends are 1.04 and 1.17 ppmv
523 decade^{-1} during the growing season and non-growing season, respectively. The model
524 simulation results suggest that domestic carbon emissions are not a main reason for the
525 observed ΔCO_2 trends.

526

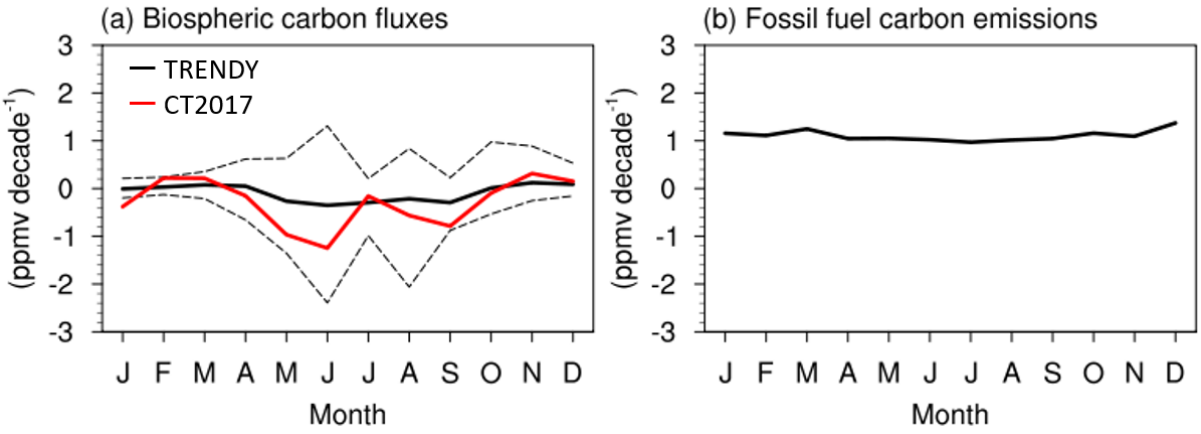

527

528 **Figure 7** Area-averaged changes in trends in monthly mean CO_2 concentrations due to (a)
529 regional terrestrial carbon fluxes (red solid line: CT2017; E1 simulation minus E3 simulation,
530 black solid and dotted lines: average, maximum, and minimum of TRENDY models' estimates;
531 T2, T3, and T4 simulations minus T1 simulation, respectively) and (b) fossil fuel carbon
532 emissions (i.e., E1 simulation minus E2 simulation) at the South Korea for the period 2000–
533 2016.

534

535 *Influences of atmospheric transport changes on CO_2 concentrations over South Korea*

536 South Korea is located in the downstream area of China, the biggest CO_2 emitter in the
537 world, and close to a strong summer uptake region (i.e. Siberia). Considering the geographical
538 location, the influences of transport changes on CO_2 concentrations over South Korea are also
539 evaluated through model simulations. Even without considering the land-surface carbon flux
540 changes in the region, annual mean CO_2 concentrations increase more than 21 ppmv decade^{-1}
541 from 2000 to 2016 over East Asia. The largest increase is found in eastern China at more than
542 31 ppmv decade^{-1} and the increasing trend is weakened further away from the region (Figure
543 8a). The spatial distributions of the increasing trends are associated with a steep rise of fossil
544 fuel carbon emissions in eastern China at 1.4 Pg C decade^{-1} for the analysis period. The

increasing carbon emissions raises CO_2 concentrations in main source regions such as the north China plain, Beijing, and Shanghai by more than 13 ppmv decade^{-1}, as well as surrounding regions including South Korea by more than 6 ppmv decade^{-1} (Figure 8b). We compared the influences of transport change on the trends of monthly mean CO_2 concentrations in the surrounding area (i.e. West Sea of Korea) and in the Korean peninsula (boxed area in Figure 8): Region1 (35–38°N, 123.0–126.0°E) and Region2 (35–38°N, 126.5–129.5°E).

The changes in atmospheric CO_2 transport raise the annual mean CO_2 concentration in Region1 more than that of in Region2 by 0.86 ppmv decade^{-1} (Figure 9a). More than 1.3 ppmv decade^{-1} of the regional differences in CO_2 concentration trends (i.e. Region2 minus Region1) are exhibited in April and November, and less than 0.5 ppmv decade^{-1} of the regional differences are found in August. The annual mean trends of the regional differences are mostly resulted from the increasing carbon emissions in eastern China (0.69 ppmv decade^{-1}; Figure 9b). The monthly variations of the regional differences are associated with wind circulation changes. For example, reduced westerly flow and northwesterly flow over the Korean Peninsula intensify the CO_2 concentration gradient from eastern China to South Korea and increase the regional differences in April and November, respectively. However, the two regions shared similar seasonal patterns in CO_2 concentration trends. Even seasonally averaged trends of the regional differences are smaller during the growing season (0.76 ppmv decade^{-1}) than that of during the non-growing season (0.95 ppmv decade^{-1}). These results suggest that the observed decreasing trend in ΔCO_2 during the growing season, distinct during the non-growing season, is not attributed to the changes in transported atmospheric CO_2 for the study period.

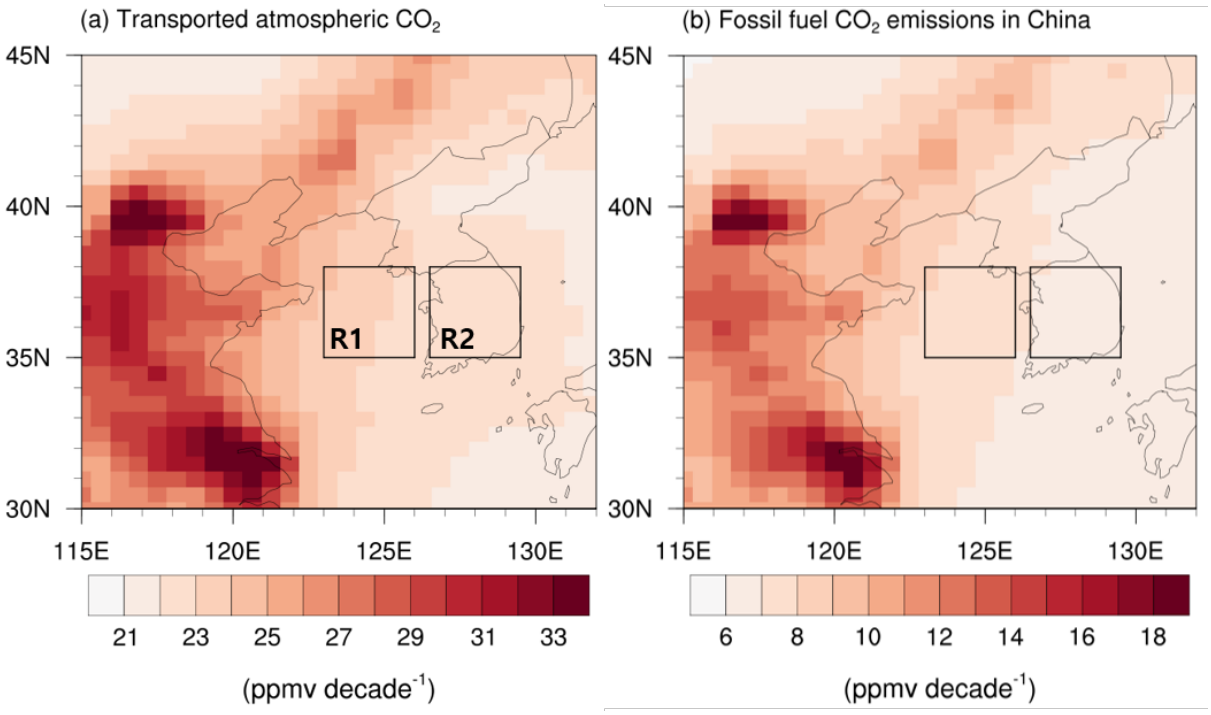

569

570 **Figure 8** Spatial distributions of changes in simulated annual mean CO_2 concentration trends
571 due to (a) transported atmospheric CO_2 (i.e. E5 simulation) and (b) China's carbon emissions
572 (i.e., E1 simulation minus E4 simulation) for the period 2000–2016.

573

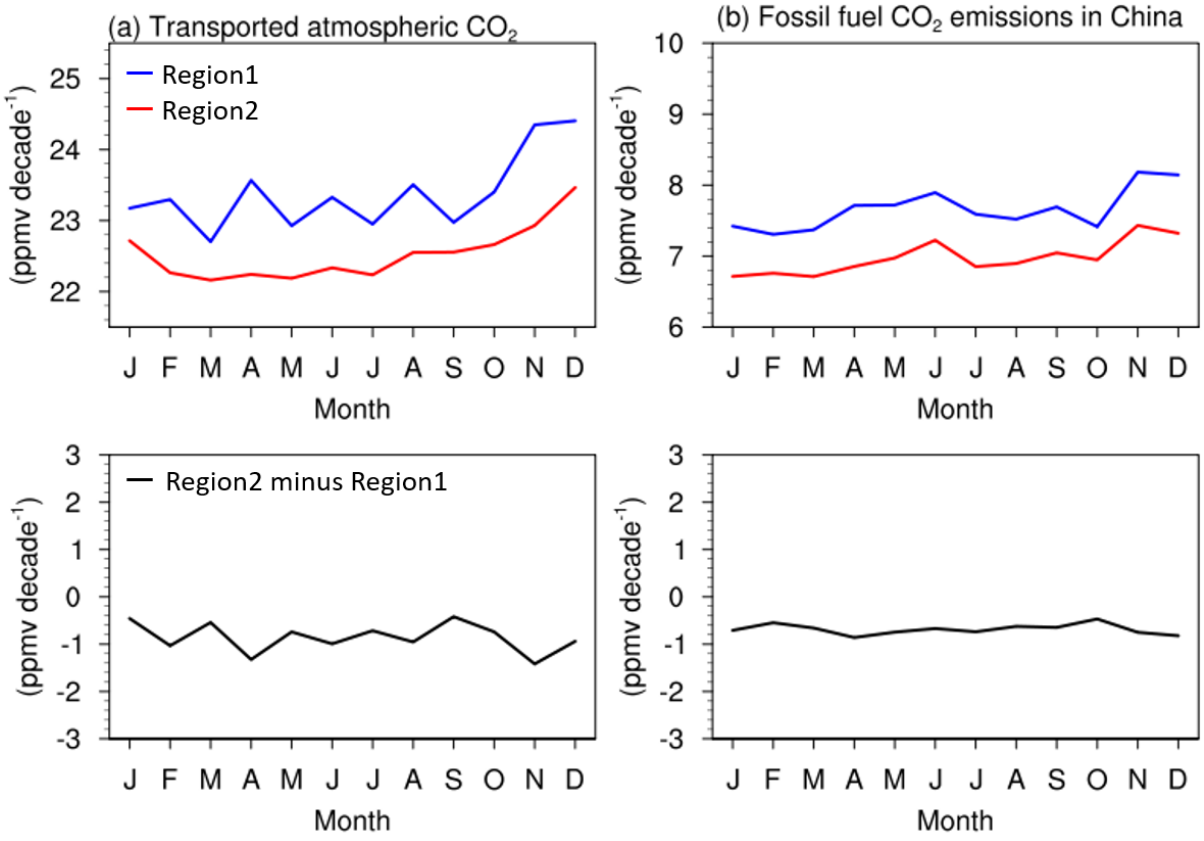

574

575 **Figure 9** Area-averaged changes in simulated monthly mean CO_2 concentration trends due to
576 (a) transported atmospheric CO_2 (i.e. E5 simulation) and (b) China's carbon emissions (i.e., E1
577 simulation minus E4 simulation) at the Region1 (35–38°N, 124.3–126.3°E), the Region2 (35–
578 38°N, 126.3–128.3°E), and the difference between them.

579

580 **Discussion**

581 The best way to understand the terrestrial carbon cycle would be to use as much
582 terrestrial carbon flux measurements as possible. However, the number of terrestrial carbon
583 flux measurements are still limited in many parts of the globe (Schimel et al., 2015). Recent
584 studies suggest the applicability of long-term measurements of atmospheric CO2
585 concentrations to evaluate the regional terrestrial carbon flux changes (Commane et al., 2016;
586 Jeong et al., 2018). This study assessed whether surface atmospheric CO_2 measurements can

be used to understand the regional terrestrial carbon cycle in South Korea. However, unlike the clean-air environment in Alaska where previous studies have been carried out (i.e., Commane et al., 2016; Jeong et al., 2018), South Korea is located at the center of the East Asia region where a rapid increase in anthropogenic carbon emissions have been reported over the recent decades (Global carbon project, 2018). The higher increasing trends of CO_2^{ocean} and CO_2^{land} than that of the globally averaged CO_2 concentration (2.07 ppmv $year^{-1}$), derived from the NOAA/ESRL data (Dlugokencky & Tans, 2019), indicate that the influences of anthropogenic emissions on the spatiotemporal variations of CO_2 concentrations cannot be negligible over the region as highlighted in previous modeling (e.g. Ballav et al., 2012; Ballav et al., 2016) and observation studies (e.g. Umezawa et al., 2018).

In this study, the changes in regional land-surface CO_2 fluxes were estimated from the difference between CO_2^{ocean} and CO_2^{land}. It is worth noting that Ballav et al. (2016) showed that the relatively high CO_2 concentration over land the night before was sometimes observed over the open ocean region the next day mostly when wind blows from land to sea; thus, higher CO_2^{land} could be observed in those cases. However, our results show that CO_2^{land} has greater seasonal variability than that of both CO_2^{ocean} (Figure 4a) and the ULD CO_2 concentrations (Figure 3) and clear seasonal variations in ΔCO_2 appeared (Figure 4b). This indicates that ΔCO_2 can capture land-surface CO_2 flux signals that are distinct from the surrounding area (i.e. the East Sea and West Sea of Korea).

Based on the observed ΔCO_2, we found that regional land carbon uptake significantly increases relative to the surrounding region during the growing season, as opposed to increase in land carbon emissions during the non-growing season. We first assumed that this was from

an increase in terrestrial carbon fluxes for the period and checked the changes in vegetation and terrestrial carbon fluxes using available satellite datasets and model simulation results. Our analysis of the satellite dataset showed that significant nationwide increasing trends in vegetation and its photosynthesis appeared for the growing season. The results are in line with the previous finding that the NDVI and vegetation production showed consistent long-term increasing trends in the region (Fang et al., 2014). The national forest inventory reporting that the forest volume of South Korea increased by 142% from 1999 to 2015 is another good evidence for the increase in vegetation production (Korea Forest Service, 2018). Generally, major reasons for the increase in vegetation growth is considered as fertilization effects of increasing ambient CO_2 and nitrogen deposition, warming-driven enhancement of photosynthesis, and lengthening of growing seasons (Jeong et al., 2013; Piao et al., 2015; Zhu et al., 2016). In addition to the environmental changes at a global scale, sustained national forest management campaigns during the last two decades seem to be another key driver. Contrasting trends in the NDVI between North and South Korea are observed in Figure 5. While forest areas in South Korea have remained steady, massive deforestation has taken place in North Korea since the early 1990s (Cui et al., 2014; Engler, Teplyakov, & Adams, 2014). The different forest management history caused a vegetation browning trend in the southern area of North Korea despite the favorable environmental conditions for vegetation growth.

In accordance with the observed increasing trend of vegetation growth and production, both TRENDY multi-model mean and CT2017 estimate the enhancement of terrestrial carbon uptake during the growing season, although the magnitudes differ by models. This study used the S3 simulation results considering all changes to climate, CO_2, and land use, but found that there were little differences in the S2 simulation results, ignoring land use change (not shown

here) despite Korean forests at least doubling in volume during the study period. It seems that the TRENDY models underestimate influences of land use change on terrestrial carbon fluxes. In addition, the globally averaged annual CO_2 concentration was equally prescribed in all regions in the TRENDY models. Considering that the increasing rate of atmospheric CO_2 at the AMY Station is higher than that of the global mean value, the CO_2 fertilization effect could also be underestimated over the region. Thus, the process-based models (i.e. TRENDY) seem to estimate the increasing trends less than that of the inverse model constrained CO_2 measurements data (i.e. CT2017). Although our CTM model simulations have relatively weaker responses to the estimated terrestrial carbon flux changes, they show that the observed ΔCO_2 decrease is associated with the enhancement of terrestrial carbon uptake in South Korea during the growing season rather than other factors (influences of other factors will be discussed in the next paragraph). The results are consistent with previous studies estimating the strengthening of the carbon sink in Korean forests based on forest inventories (Pan et al., 2011; Jeong et al., 2013; Fang et al., 2014). Therefore, our findings provide an evidence that atmospheric CO_2 measurements could be used to detect changes in the terrestrial carbon cycle at regional scales even where anthropogenic activities are not treated as minimal components.

This study suggests that increase in terrestrial carbon uptake is a key process causing changes in temporal variations of ΔCO_2. However, ΔCO_2 variations can also be modulated by fossil fuel carbon emissions and atmospheric circulation changes. From the CTM model simulations, we checked all the potential influences of the factors. The model estimates that the increase in domestic fossil fuel carbon emissions do not make notable seasonal differences in the CO_2 concentration trends in South Korea. That is because seasonal variability of the carbon emissions trends is relatively too small than that of terrestrial carbon fluxes, which

659 change its sign in the growing season and non-growing season. Previous studies also show that
660 the fossil fuel carbon emissions in main source regions have around 20% of seasonal variability
661 of biospheric carbon fluxes over the tropics and northern middle latitude (Zhang, Gurney,
662 Rayner, Baker, & Liu, 2016). Even with the small seasonal variability, our results show that
663 the increasing carbon emissions in China, which is more than 40 times of that in South Korea,
664 has potential to make around 1 ppmv decade^{-1} annual amplitude of increasing rates of CO_2
665 concentrations over South Korea. However, because the seasonal patterns of CO_2 concentration
666 trends are similar around and in the Korean Peninsula, China's emissions also seem to be a
667 minor factor on the long-term trends in the seasonal cycle of ΔCO_2. One thing to keep in mind
668 is that the greater increasing rate of CO_2 concentrations in the West Sea of Korea than the
669 Korean Peninsula could alleviate the ΔCO_2 increase caused by the increasing domestic carbon
670 emissions. Readers need to be cautious when interpreting our results (i.e. decrease in annual
671 ΔCO_2 trends does not mean that South Korea becomes a net carbon sink). We also found that
672 the atmospheric circulation changes have possibilities to induce unequal temporal changes in
673 CO_2 concentrations over South Korea. Our model suggests, however, that there are no notable
674 changes in atmospheric circulation patterns that lead to the observed ΔCO_2 trend for the study
675 period. This study treated the anthropogenic emissions and atmospheric circulation as main
676 drivers of transport changes, but the enhancement of terrestrial carbon uptake in boreal forests,
677 highlighted in previous studies (Graven et al., 2013; Welp et al., 2016), can also be another
678 driver. Welp et al. (2016) showed that significant increases in biospheric CO_2 flux appeared in
679 boreal regions at 0.35% year^{-1} and in arctic regions at 0.85 % year^{-1} for the period 1982–2012
680 from inversion results. We evaluated the possible effect through a set of ideal model
681 experiments with and without a 1% year^{-1} increase in seasonal amplitude of monthly terrestrial
682 CO_2 fluxes in high-latitude regions (>45°N) for the study period. The model estimated that the
683 increasing biospheric carbon uptake increases the seasonal amplitude of CO_2 concentration

around 1.6 ppmv decade^{-1} over South Korea, but it also did not make remarkable regional differences in the CO_2 concentration trends around the region (not shown here).

This study takes the advantages of the long-term continuous CO_2 measurement at the AMY Station. In addition to the AMY Station, numerous surface stations are continuously measuring atmospheric CO_2 concentration over the globe and provides hourly data. Because many of these observation sites are located on the coastal side, our approach has potential to provide wide-area information. Even if the station is located far from the coast, we could retrieve signals of terrestrial carbon exchange by considering physical characteristics of local wind circulation. For example, the Mauna Loa Observatory (MLO), located at a high altitude (3397m) in the center of the Hawaiian Islands, observes CO_2 concentrations above the planetary boundary layer, but CO_2 concentrations are affected by the airflow blowing from lower altitudes to the site during a few hours after sunset (Sharma and Barnes, 2016). The difference of observed CO_2 concentration between the two periods could play the role of ΔCO_2 of this study. In addition, local variations in land carbon flux within the continent could be detected from a comparison of atmospheric CO_2 data from adjacent observation sites (e.g. Sargent et al., 2018).

In summary, this study showed that the terrestrial carbon uptake has been enhanced resulted from the nationwide vegetation greening over South Korea during the growing season for the past two decades based on multiple lines of evidence from atmospheric measurements, satellite observations, and model simulations. Additional surface observation sites have been operated in the mainland (e.g. Seoul) and test operations for long-term aircraft measurements across the Korean Peninsula have been conducted since 2018. Satellites like the Greenhouse

gases Observing SATellite (GOSAT), Orbiting Carbon Observatory 2 (OCO-2), and TanSat also have measured a large spatial extent of column-averaged CO_2 concentrations. Inverse modeling using the added in situ, airborne, and satellite data would provide more reliable quantitative information on the increase in terrestrial carbon uptake by using the relationship between our results (i.e. ΔCO_2) and the estimated biosphere flux in future studies (e.g. Commane et al., 2016). Atmospheric CO_2 measurements could open up the possibility for a better understanding of the terrestrial carbon cycle where ground-based observation is limited; therefore, sustained efforts to expand the observation network are required.

Acknowledgements

This study was supported by the Korea Meteorological Administration Research and Development Program under grant KMI2018-03711 and the National Research Foundation of Korea (NRF) grant funded by the Korean government (MSIT) (No. NRF-2019R1A2C3002868). Chang-Hoi Ho was funded by the Korea Ministry of Environment as part of the Climate Change Correspondence Program. Vanessa Haverd was supported from the Earth Systems and Climate Change Hub, funded by the Australian Government's National Environmental Science Program. The data at AMY was from the project funded by the Korea Meteorological Administration Research and Development Program "Research and Development for KMA Weather, Climate, and Earth system Services – Development of Monitoring and Analysis Techniques for Atmospheric Composition in Korea" under grant 1365003041.

References

731 Baker, D. F., Law, R. M., Gurney, K. R., Rayner, P., Peylin, P., Denning, A. S., … Zhu, Z.
732 (2006). TransCom 3 inversion intercomparison: Impact of transport model errors on the
733 interannual variability of regional CO2 fluxes, 1988–2003. *Global Biogeochemical Cycles*,
734 *20*(1). https://doi.org/10.1029/2004GB002439
735 Ballav, S., Patra, P. K., Sawa, Y., Matsueda, H., Adachi, A., Onogi, S., … De, U. K. (2016).
736 Simulation of CO 2 concentrations at Tsukuba tall tower using WRF-CO 2 tracer transport
737 model. *Journal of Earth System Science*, *125*(1), 47–64. https://doi.org/10.1007/s12040-
738 015-0653-y
739 Ballav, S., Patra, P. K., Takigawa, M., Ghosh, S., De, U. K., Maksyutov, S., … Hashimoto, S.
740 (2012). Simulation of CO2 concentration over East Asia using the regional transport model
741 WRF-CO2. *Journal of the Meteorological Society of Japan. Ser. II*, *90*(6), 959–976.
742 https://doi.org/10.2151/jmsj.2012-607
743 Barnes, E. A., Parazoo, N., Orbe, C., & Denning, A. S. (2016). Isentropic transport and the
744 seasonal cycle amplitude of CO2. *Journal of Geophysical Research: Atmospheres*, *121*(13),
745 2016JD025109. https://doi.org/10.1002/2016JD025109
746 Bey, I., Jacob, D. J., Yantosca, R. M., Logan, J. A., Field, B. D., Fiore, A. M., … Schultz, M.
747 G. (2001). Global modeling of tropospheric chemistry with assimilated meteorology:
748 Model description and evaluation. *Journal of Geophysical Research: Atmospheres*,
749 *106*(D19), 23073–23095. https://doi.org/10.1029/2001JD000807
750 Bruhwiler, L. M. P., Michalak, A. M., & Tans, P. P. (2011). Spatial and temporal resolution of
751 carbon flux estimates for 1983–2002. *Biogeosciences*, *8*(5), 1309–1331.
752 https://doi.org/10.5194/bg-8-1309-2011
753 Canadell, J. G., Ciais, P., Gurney, K., Quéré, C. L., Piao, S., Raupach, M. R., & Sabine, C. L.
754 (2011). An international effort to quantify regional carbon fluxes. *Eos, Transactions*
755 *American Geophysical Union*, *92*(10), 81–82. https://doi.org/10.1029/2011EO100001

Cho, C.-H., Kim, J.-S., & Yoo, H.-J. (2007). Atmospheric carbon dioxide variations at Korea GAW center from 1999 to 2006. *Asia-Pacific Journal of Atmospheric Sciences*, *43*(4), 359–365.

Choi, S.-D., Lee, K., & Chang, Y.-S. (2002). Large rate of uptake of atmospheric carbon dioxide by planted forest biomass in Korea. *Global Biogeochemical Cycles*, *16*(4), 1089. https://doi.org/10.1029/2002GB001914

Clark, D. B., Mercado, L. M., Sitch, S., Jones, C. D., Gedney, N., Best, M. J., … Cox, P. M. (2011). The Joint UK Land Environment Simulator (JULES), model description – Part 2: Carbon fluxes and vegetation dynamics. *Geoscientific Model Development*, *4*(3), 701–722. https://doi.org/10.5194/gmd-4-701-2011

Commane, R., Lindaas, J., Benmergui, J., Luus, K. A., Chang, R. Y.-W., Daube, B. C., … Wofsy, S. C. (2017). Carbon dioxide sources from Alaska driven by increasing early winter respiration from Arctic tundra. *Proceedings of the National Academy of Sciences*, *114*(21), 5361–5366. https://doi.org/10.1073/pnas.1618567114

Cui, G., Lee, W.-K., Kim, D., Lee, E. J., Kwak, H., Choi, H.-A., … Jeon, S. (2014). Estimation of forest carbon budget from land cover change in South and North Korea between 1981 and 2010. *Journal of Plant Biology*, *57*(4), 225–238. https://doi.org/10.1007/s12374-014-0165-3

Didan, K. (2015). MOD13Q1 MODIS/Terra vegetation indices 16-day L3 global 250m SIN grid V006. *NASA EOSDIS Land Processes DAAC*.

Dlugokencky, E. & Tans, P. (2019). Trends in global CO_2, National Oceanic & Atmospheric Administration, Earth System Research Laboratory (NOAA/ESRL), available at http://www.esrl.noaa.gov/gmd/ccgg/trends.

779 Dragoni, D., Schmid, H. P., Wayson, C. A., Potter, H., Grimmond, C. S. B., & Randolph, J. C.
780 (2011). Evidence of increased net ecosystem productivity associated with a longer
781 vegetated season in a deciduous forest in south-central Indiana, USA. *Global Change*
782 *Biology*, *17*(2), 886–897. https://doi.org/10.1111/j.1365-2486.2010.02281.x
783 Engler, R., Teplyakov, V., & Adams, J. M. (2014). An assessment of forest cover trends in
784 South and North Korea, from 1980 to 2010. *Environmental Management*, *53*(1), 194–201.
785 https://doi.org/10.1007/s00267-013-0201-y
786 Enting, I. G., & Mansbridge, J. V. (1989). Seasonal sources and sinks of atmospheric CO2
787 Direct inversion of filtered data. *Tellus B: Chemical and Physical Meteorology*, *41*(2), 111–
788 126. https://doi.org/10.3402/tellusb.v41i2.15056
789 Fang, J., Guo, Z., Hu, H., Kato, T., Muraoka, H., & Son, Y. (2014). Forest biomass carbon sinks
790 in East Asia, with special reference to the relative contributions of forest expansion and
791 forest growth. *Global Change Biology*, *20*(6), 2019–2030.
792 https://doi.org/10.1111/gcb.12512
793 Gelaro, R., McCarty, W., Suárez, M. J., Todling, R., Molod, A., Takacs, L., … Zhao, B. (2017).
794 The Modern-Era Retrospective Analysis for Research and Applications, Version 2
795 (MERRA-2). *Journal of Climate*, *30*(14), 5419–5454. https://doi.org/10.1175/JCLI-D-16-
796 0758.1
797 Global Carbon Project (2018). Supplemental data of Global Carbon Budget 2018 (Version 1.0)
798 [2018 National Emissions v1.0], available at https://www.icos-cp.eu/GCP/2018.
799 Graven, H. D., Keeling, R. F., Piper, S. C., Patra, P. K., Stephens, B. B., Wofsy, S. C., … Bent,
800 J. D. (2013). Enhanced seasonal exchange of CO2 by northern ecosystems since 1960.
801 *Science*, *341*(6150), 1085–1089. https://doi.org/10.1126/science.1239207

Gurney, K. R., Law, R. M., Denning, A. S., Rayner, P. J., Baker, D., Bousquet, P., … Yuen, C.-W. (2003). TransCom 3 CO2 inversion intercomparison: 1. Annual mean control results and sensitivity to transport and prior flux information. *Tellus B: Chemical and Physical Meteorology*, *55*(2), 555–579. https://doi.org/10.3402/tellusb.v55i2.16728

Haverd, V., Smith, B., Nieradzik, L., Briggs, P. R., Woodgate, W., Trudinger, C. M., ... Cuntz, M. (2018). A new version of the CABLE land surface model (Subversion revision r4601) incorporating land use and land cover change, woody vegetation demography, and a novel optimisation-based approach to plant coordination of photosynthesis. *Geoscientific Model Development*, *11*(7), 2995-3026. https://doi.org/10.5194/gmd-11-2995-2018

Huntzinger, D. N., Post, W. M., Wei, Y., Michalak, A. M., West, T. O., Jacobson, A. R., ... Cook, R. (2012). North American Carbon Program (NACP) regional interim synthesis: Terrestrial biospheric model intercomparison. *Ecological Modelling*, *232*, 144-157. https://doi.org/10.1016/j.ecolmodel.2012.02.004

Hurtt, G. C., Chini, L. P., Frolking, S., Betts, R. A., Feddema, J., Fischer, G., ... Wang, Y. P. (2011). Harmonization of land-use scenarios for the period 1500–2100: 600 years of global gridded annual land-use transitions, wood harvest, and resulting secondary lands. *Climatic change*, *109*(1-2), 117. https://doi.org/10.1007/s10584-011-0153-2

IPCC. (2014). Climate change 2014: *synthesis report. Contribution of Working Groups I, II and III to the fifth assessment report of the Intergovernmental Panel on Climate Change* (pp. 77-78) [Core Writing Team, R.K. Pachauri & L.A. Meyer (eds.)], IPCC, Geneva, Switzerland, 151 pp.

Ito, A., & Inatomi, M. (2012). Use of a process-based model for assessing the methane budgets of global terrestrial ecosystems and evaluation of uncertainty. *Biogeosciences*, *9*(2), 759–773. https://doi.org/10.5194/bg-9-759-2012

826 Jain, A. K., Meiyappan, P., Song, Y., & House, J. I. (2013). CO_2 emissions from land-use
827 change affected more by nitrogen cycle, than by the choice of land-cover data. *Global*
828 *Change Biology*, *19*(9), 2893–2906. https://doi.org/10.1111/gcb.12207

829 Jeong, S.-J., Bloom, A. A., Schimel, D., Sweeney, C., Parazoo, N. C., Medvigy, D., … Miller,
830 C. E. (2018). Accelerating rates of Arctic carbon cycling revealed by long-term
831 atmospheric CO2 measurements. *Science Advances*, *4*(7), eaao1167.
832 https://doi.org/10.1126/sciadv.aao1167

833 Jeong, S.-J., Ho, C.-H., Choi, S.-D., Kim, J., Lee, E.-J., & Gim, H.-J. (2013). Satellite data-
834 based phenological evaluation of the nationwide reforestation of South Korea. *PLOS ONE*,
835 *8*(3), e58900. https://doi.org/10.1371/journal.pone.0058900

836 Jeong, S.-J., Ho, C.-H., & Jeong, J.-H. (2009). Increase in vegetation greenness and decrease
837 in springtime warming over east Asia. *Geophysical Research Letters*, *36*(2), L02710.
838 https://doi.org/10.1029/2008GL036583

839 Joos, F., & Spahni, R. (2008). Rates of change in natural and anthropogenic radiative forcing
840 over the past 20,000 years. *Proceedings of the National Academy of Sciences*, *105*(5),
841 1425–1430. https://doi.org/10.1073/pnas.0707386105

842 Keenan, T. F., Gray, J., Friedl, M. A., Toomey, M., Bohrer, G., Hollinger, D. Y., … Richardson,
843 A. D. (2014). Net carbon uptake has increased through warming-induced changes in
844 temperate forest phenology. *Nature Climate Change*, *4*(7), 598–604.
845 https://doi.org/10.1038/nclimate2253

846 Korea Forest Service (2018) Statistical yearbook of forest. Korea Forest Service, Seoul,
847 Republic of Korea.

848 Krinner, G., Viovy, N., Noblet-Ducoudré, N. de, Ogée, J., Polcher, J., Friedlingstein, P., …

Prentice, I. C. (2005). A dynamic global vegetation model for studies of the coupled atmosphere-biosphere system. *Global Biogeochemical Cycles*, *19*(1). https://doi.org/10.1029/2003GB002199

Le Quéré, C., Andrew, R. M., Friedlingstein, P., Sitch, S., Hauck, J., Pongratz, J., ... & Zheng, B. (2018). Global carbon budget 2018. *Earth System Science Data (Online)*, *10*(4). https://doi.org/10.5194/essd-10-2141-2018

Lee, H., Han, S.-O., Ryoo, S.-B., Lee, J.-S., & Lee, G.-W. (2019). The measurement of atmospheric CO_2 at KMA GAW regional stations, its characteristics, and comparisons with other East Asian sites. *Atmospheric Chemistry and Physics*, *19*(4), 2149–2163. https://doi.org/10.5194/acp-19-2149-2019

Lee, J.-Y., Kwon, M., Yun, K.-S., Min, S.-K., Park, I.-H., Ham, Y.-G., … Yoon, J.-H. (2017). The long-term variability of Changma in the East Asian summer monsoon system: A review and revisit. *Asia-Pacific Journal of Atmospheric Sciences*, *53*(2), 257–272. https://doi.org/10.1007/s13143-017-0032-5

Lee, J., Yoon, T. K., Han, S., Kim, S., Yi, M. J., Park, G. S., … Son, Y. (2014). Estimating the carbon dynamics of South Korean forests from 1954 to 2012. *Biogeosciences*, *11*(17), 4637–4650. https://doi.org/10.5194/bg-11-4637-2014

Li, X., Yi, M. J., Son, Y., Jin, G., & Han, S. S. (2010). Forest biomass carbon accumulation in Korea from 1954 to 2007. *Scandinavian Journal of Forest Research*, *25*(6), 554–563. https://doi.org/10.1080/02827581.2010.524892

Liu, J., Bowman, K. W., Lee, M., Henze, D. K., Bousserez, N., Brix, H., … Nassar, R. (2014). Carbon monitoring system flux estimation and attribution: impact of ACOS-GOSAT XCO2 sampling on the inference of terrestrial biospheric sources and sinks. *Tellus B:*

872 *Chemical and Physical Meteorology*, *66*(1), 22486.
873 https://doi.org/10.3402/tellusb.v66.22486

874 Messerschmidt, J., Parazoo, N., Wunch, D., Deutscher, N. M., Roehl, C., Warneke, T., &
875 Wennberg, P. O. (2013). Evaluation of seasonal atmosphere–biosphere exchange
876 estimations with TCCON measurements. *Atmospheric Chemistry and Physics*, *13*(10),
877 5103–5115. https://doi.org/10.5194/acp-13-5103-2013

878 Min, S.-K., Zhang, X., Zwiers, F. W., & Hegerl, G. C. (2011). Human contribution to more-
879 intense precipitation extremes. *Nature*, *470*(7334), 378–381.
880 https://doi.org/10.1038/nature09763

881 MODIS Land Team. (2018). Status for: Vegetation Indices (MOD13), online:
882 https://landval.gsfc.nasa.gov/ProductStatus.php?ProductID=MOD13

883 Nassar, R., Napier-Linton, L., Gurney, K. R., Andres, R. J., Oda, T., Vogel, F. R., & Deng, F.
884 (2013). Improving the temporal and spatial distribution of CO2 emissions from global
885 fossil fuel emission data sets. *Journal of Geophysical Research: Atmospheres*, *118*(2),
886 917–933. https://doi.org/10.1029/2012JD018196

887 Nassar, R., Jones, D. B. A., Kulawik, S. S., Worden, J. R., Bowman, K. W., Andres, R. J., …
888 Worthy, D. E. (2011). Inverse modeling of CO_2 sources and sinks using satellite
889 observations of CO_2 from TES and surface flask measurements. *Atmospheric Chemistry*
890 *and Physics*, *11*(12), 6029–6047. https://doi.org/10.5194/acp-11-6029-2011

891 Oda, T., & Maksyutov, S. (2011). A very high-resolution (1 km×1 km) global fossil fuel CO2
892 emission inventory derived using a point source database and satellite observations of
893 nighttime lights. *Atmos. Chem. Phys.*, *11*(2), 543–556. https://doi.org/10.5194/acp-11-543-
894 2011

Oleson, K. W., Lawrence, D. M., Gordon, B., Flanner, M. G., Kluzek, E., Peter, J., …Heald, C. L. (2013). Technical description of version 4.5 of the Community Land Model (CLM), NCAR Technical Note NCAR/TN-503+STR. 420 pp.

Pan, Y., Birdsey, R. A., Fang, J., Houghton, R., Kauppi, P. E., Kurz, W. A., … Hayes, D. (2011). A large and persistent carbon sink in the world's forests. *Science*, *333*(6045), 988–993. https://doi.org/10.1126/science.1201609

Parazoo, N. C., Commane, R., Wofsy, S. C., Koven, C. D., Sweeney, C., Lawrence, D. M., … Miller, C. E. (2016). Detecting regional patterns of changing CO2 flux in Alaska. *Proceedings of the National Academy of Sciences*, *113*(28), 7733–7738. https://doi.org/10.1073/pnas.1601085113

Patra, P. K., Niwa, Y., Schuck, T. J., Brenninkmeijer, C. a. M., Machida, T., Matsueda, H., & Sawa, Y. (2011). Carbon balance of South Asia constrained by passenger aircraft CO_2 measurements. *Atmospheric Chemistry and Physics*, *11*(9), 4163–4175. https://doi.org/10.5194/acp-11-4163-2011

Peters, W., Jacobson, A. R., Sweeney, C., Andrews, A. E., Conway, T. J., Masarie, K., … Tans, P. P. (2007). An atmospheric perspective on North American carbon dioxide exchange: CarbonTracker. *Proceedings of the National Academy of Sciences*, *104*(48), 18925–18930. https://doi.org/10.1073/pnas.0708986104

Peylin, P., Law, R. M., Gurney, K. R., Chevallier, F., Jacobson, A. R., Maki, T., … Zhang, X. (2013). Global atmospheric carbon budget: Results from an ensemble of atmospheric CO2 inversions. *Biogeosciences*, *10*, 6699–6720. https://doi.org/10.5194/bg-10-6699-2013

Piao, S., Yin, G., Tan, J., Cheng, L., Huang, M., Li, Y., … Wang, Y. (2015). Detection and attribution of vegetation greening trend in China over the last 30 years. *Global Change Biology*, *21*(4), 1601–1609. https://doi.org/10.1111/gcb.12795

Piao, S., Sitch, S., Ciais, P., Friedlingstein, P., Peylin, P., Wang, X., … Zeng, N. (2013). Evaluation of terrestrial carbon cycle models for their response to climate variability and to CO2 trends. *Global Change Biology*, *19*(7), 2117–2132. https://doi.org/10.1111/gcb.12187

Piao, S. L., Ito, A., Li, S. G., Huang, Y., Ciais, P., Wang, X. H., … Zhu, B. (2012). The carbon budget of terrestrial ecosystems in East Asia over the last two decades. *Biogeosciences*, *9*(9), 3571–3586. https://doi.org/10.5194/bg-9-3571-2012

Piao, S., Ciais, P., Lomas, M., Beer, C., Liu, H., Fang, J., … Woodward, I. (2011). Contribution of climate change and rising CO2 to terrestrial carbon balance in East Asia: A multi-model analysis. *Global and Planetary Change*, *75*(3), 133–142. https://doi.org/10.1016/j.gloplacha.2010.10.014

Piao, S., Ciais, P., Friedlingstein, P., Peylin, P., Reichstein, M., Luyssaert, S., … Vesala, T. (2008). Net carbon dioxide losses of northern ecosystems in response to autumn warming. *Nature*, *451*(7174), 49–52. https://doi.org/10.1038/nature06444

Pinzon, J. E., & Tucker, C. J. (2014). A non-stationary 1981–2012 AVHRR NDVI3g time series. *Remote Sensing*, *6*(8), 6929–6960. https://doi.org/10.3390/rs6086929

Randerson, J. T., Van Der Werf, G. R., Giglio, L., Collatz, G. J., & Kasibhatla, P. S. (2018). Global Fire Emissions Database, Version 4, (GFEDv4). ORNL DAAC, Oak Ridge, Tennessee, USA, available at https://doi.org/10.3334/ORNLDAAC/1293

Sargent, M., Barrera, Y., Nehrkorn, T., Hutyra, L. R., Gately, C. K., Jones, T., … Wofsy, S. C. (2018). Anthropogenic and biogenic CO2 fluxes in the Boston urban region. *Proceedings of the National Academy of Sciences*, *115*(29), 7491–7496. https://doi.org/10.1073/pnas.1803715115

Schimel, D., Pavlick, R., Fisher, J. B., Asner, G. P., Saatchi, S., Townsend, P., … Cox, P. (2015). Observing terrestrial ecosystems and the carbon cycle from space. *Global Change Biology*, *21*(5), 1762–1776. https://doi.org/10.1111/gcb.12822

Seneviratne, S. I., Donat, M. G., Pitman, A. J., Knutti, R., & Wilby, R. L. (2016). Allowable CO2 emissions based on regional and impact-related climate targets. *Nature*, *529*(7587), 477–483. https://doi.org/10.1038/nature16542

Sharma, N. C. P., & Barnes, J. E. (2016). Boundary layer characteristics over a high altitude station, Mauna Loa Observatory. *Aerosol and Air Quality Research*, *16*(3), 729–737. https://doi.org/10.4209/aaqr.2015.05.0347

Simone, N. W., Stettler, M. E. J., & Barrett, S. R. H. (2013). Rapid estimation of global civil aviation emissions with uncertainty quantification. *Transportation Research Part D: Transport and Environment*, *25*, 33–41. https://doi.org/10.1016/j.trd.2013.07.001

Sitch, S., Friedlingstein, P., Gruber, N., Jones, S. D., Murray-Tortarolo, G., Ahlström, A., … Myneni, R. (2015). Recent trends and drivers of regional sources and sinks of carbon dioxide. *Biogeosciences*, *12*(3), 653–679. https://doi.org/10.5194/bg-12-653-2015

Sitch, S., Smith, B., Prentice, I. C., Arneth, A., Bondeau, A., Cramer, W., … Venevsky, S. (2003). Evaluation of ecosystem dynamics, plant geography and terrestrial carbon cycling in the LPJ dynamic global vegetation model. *Global Change Biology*, *9*(2), 161–185. https://doi.org/10.1046/j.1365-2486.2003.00569.x

Stein, A. F., Draxler, R. R., Rolph, G. D., Stunder, B. J. B., Cohen, M. D., & Ngan, F. (2015). NOAA's HYSPLIT atmospheric transport and dispersion modeling system. *Bulletin of the American Meteorological Society*, *96*(12), 2059–2077. https://doi.org/10.1175/BAMS-D-14-00110.1

Stocker, B. D., Feissli, F., Strassmann, K. M., Spahni, R., & Joos, F. (2014). Past and future

carbon fluxes from land use change, shifting cultivation and wood harvest. *Tellus B: Chemical and Physical Meteorology*, *66*(1), 23188. https://doi.org/10.3402/tellusb.v66.23188

Sweeney, C., Dlugokencky, E., Miller, C. E., Wofsy, S., Karion, A., Dinardo, S., … Tans, P. (2016). No significant increase in long-term CH4 emissions on North Slope of Alaska despite significant increase in air temperature. *Geophysical Research Letters*, *43*(12), 2016GL069292. https://doi.org/10.1002/2016GL069292

Takahashi, T., Sutherland, S. C., Wanninkhof, R., Sweeney, C., Feely, R. A., Chipman, D. W., … de Baar, H. J. W. (2009). Climatological mean and decadal change in surface ocean pCO2, and net sea–air CO2 flux over the global oceans. *Deep Sea Research Part II: Topical Studies in Oceanography*, *56*(8), 554–577. https://doi.org/10.1016/j.dsr2.2008.12.009

Thompson, R. L., Patra, P. K., Chevallier, F., Maksyutov, S., Law, R. M., Ziehn, T., … Ciais, P. (2016). Top–down assessment of the Asian carbon budget since the mid 1990s. *Nature Communications*, *7*, 10724. https://doi.org/10.1038/ncomms10724

Thoning, K. W., Tans, P. P., & Komhyr, W. D. (1989). Atmospheric carbon dioxide at Mauna Loa Observatory: 2. Analysis of the NOAA GMCC data, 1974–1985. *Journal of Geophysical Research: Atmospheres*, *94*(D6), 8549–8565. https://doi.org/10.1029/JD094iD06p08549

Tian, H., Chen, G., Lu, C., Xu, X., Hayes, D. J., Ren, W., … Wofsy, S. C. (2015). North American terrestrial CO2 uptake largely offset by CH4 and N2O emissions: toward a full accounting of the greenhouse gas budget. *Climatic Change*, *129*(3), 413–426. https://doi.org/10.1007/s10584-014-1072-9

989 Umezawa, T., Matsueda, H., Sawa, Y., Niwa, Y., Machida, T., & Zhou, L. (2018). Seasonal
990 evaluation of tropospheric CO2 over the Asia-Pacific region observed by the CONTRAIL
991 commercial airliner measurements. *Atmospheric Chemistry and Physics Discussions*, 1–
992 28. https://doi.org/10.5194/acp-2018-519
993 Wang, Y. X., McElroy, M. B., Jacob, D. J., & Yantosca, R. M. (2004). A nested grid formulation
994 for chemical transport over Asia: Applications to CO. *Journal of Geophysical Research:*
995 *Atmospheres*, *109*(D22). https://doi.org/10.1029/2004JD005237
996 Welp, L. R., Patra, P. K., Rödenbeck, C., Nemani, R., Bi, J., Piper, S. C., & Keeling, R. F.
997 (2016). Increasing summer net CO_2 uptake in high northern ecosystems inferred from
998 atmospheric inversions and comparisons to remote-sensing NDVI. *Atmospheric Chemistry*
999 *and Physics*, *16*(14), 9047–9066. https://doi.org/10.5194/acp-16-9047-2016
1000 World Bank. (2018). GDP per capita (current US$). Washington, D.C., The World Bank
1001 Online: https://data.worldbank.org/indicator/NY.GDP.MKTP.CD?locations=KR
1002 Yevich, R., & Logan, J. A. (2003). An assessment of biofuel use and burning of agricultural
1003 waste in the developing world. *Global Biogeochemical Cycles*, *17*(4), n/a-n/a.
1004 https://doi.org/10.1029/2002GB001952
1005 Yue, X., Unger, N., & Zheng, Y. (2015). Distinguishing the drivers of trends in land carbon
1006 fluxes and plant volatile emissions over the past 3 decades. *Atmos. Chem. Phys.*, *15*(20),
1007 11931–11948. https://doi.org/10.5194/acp-15-11931-2015
1008 Yun, S. J., & Chun, J. (2018). Long-term ecological research on Korean forest ecosystems: the
1009 current status and challenges. *Ecological Research*, *33*(6), 1289–1302.
1010 https://doi.org/10.1007/s11284-018-1645-6
1011 Zaehle, S., Friedlingstein, P., & Friend, A. D. (2010). Terrestrial nitrogen feedbacks may
1012 accelerate future climate change. *Geophysical Research Letters*, *37*(1).

https://doi.org/10.1029/2009GL041345

Zeng, N., Mariotti, A., & Wetzel, P. (2005). Terrestrial mechanisms of interannual CO2 variability. *Global Biogeochemical Cycles*, *19*(1). https://doi.org/10.1029/2004GB002273

Zhang, Y., Song, C., Band, L. E., Sun, G., & Li, J. (2017). Reanalysis of global terrestrial vegetation trends from MODIS products: Browning or greening? *Remote Sensing of Environment*, *191*, 145–155. https://doi.org/10.1016/j.rse.2016.12.018

Zhang, X., Gurney, K. R., Rayner, P., Baker, D., & Liu, Y.-P. (2016). Sensitivity of simulated CO2 concentration to sub-annual variations in fossil fuel CO2 emissions. *Atmos. Chem. Phys.*, *16*(4), 1907–1918. https://doi.org/10.5194/acp-16-1907-2016

Zhou, L., Tucker, C. J., Kaufmann, R. K., Slayback, D., Shabanov, N. V., & Myneni, R. B. (2001). Variations in northern vegetation activity inferred from satellite data of vegetation index during 1981 to 1999. *Journal of Geophysical Research: Atmospheres*, *106*(D17), 20069–20083. https://doi.org/10.1029/2000JD000115

Zhu, Z., Piao, S., Myneni, R. B., Huang, M., Zeng, Z., Canadell, J. G., … Zeng, N. (2016). Greening of the Earth and its drivers. *Nature Climate Change*, *6*(8), 791–795. https://doi.org/10.1038/nclimate3004